HEALTH AND MEDICINE

# Blood-brain barrier–penetrating siRNA nanomedicine for Alzheimer's disease therapy

**Yutong Zhou[1]*, Feiyan Zhu[2]*, Yang Liu[2,3]*, Meng Zheng[2†], Yibin Wang[2], Dongya Zhang[2], Yasutaka Anraku[4], Yan Zou[2,5], Jia Li[3], Haigang Wu[2], Xiaobin Pang[3], Wei Tao[6], Olga Shimoni[7], Ashley I. Bush[8], Xue Xue[1†], Bingyang Shi[2,5†]**



**Toxic aggregated amyloid-β accumulation is a key pathogenic event in Alzheimer's disease (AD), which derives from amyloid precursor protein (APP) through sequential cleavage by BACE1 (β-site APP cleavage enzyme 1) and γ-secretase. Small interfering RNAs (siRNAs) show great promise for AD therapy by specific silencing of BACE1. However, lack of effective siRNA brain delivery approaches limits this strategy. Here, we developed a glycosylated "triple-interaction" stabilized polymeric siRNA nanomedicine (Gal-NP@siRNA) to target BACE1 in APP/PS1 transgenic AD mouse model. Gal-NP@siRNA exhibits superior blood stability and can efficiently penetrate the blood-brain barrier (BBB) via glycemia-controlled glucose transporter-1 (Glut1)–mediated transport, thereby ensuring that siRNAs decrease BACE1 expression and modify relative pathways. Noticeably, Gal-NP@siBACE1 administration restored the deterioration of cognitive capacity in AD mice without notable side effects. This "Trojan horse" strategy supports the utility of RNA interference therapy in neurodegenerative diseases.**

## INTRODUCTION

Alzheimer's disease (AD) is the most common age-related neurodegenerative disorder, characterized by progressive deterioration of cognitive capacity (*1*). In 2019, AD affected more than 50 million people globally, which is expected to reach 152 million by 2050 (*2*). In addition, the current annual cost of AD worldwide is $1 trillion, which is estimated to double by 2030 (*2*). Currently, clinical therapy using acetylcholinesterase inhibitors or *N*-methyl-D-aspartate receptor antagonists are palliative treatment options, which only moderately improve cognition and behavior in Alzheimer's patients but do not slow disease progression (*3*, *4*). Hence, it is imperative to develop therapeutics targeting pathological mechanisms in AD.

The precise pathological mechanisms leading to AD are not fully understood. However, plaques composed of aggregated amyloid-β peptide (Aβ), neurofibrillary tangles containing hyperphosphorylated tau protein, and neuroinflammation are pathological hallmarks (*5*). Among these, the aberrant accumulation of Aβ resulting from the sequential cleavage of the amyloid precursor protein (APP) by BACE1 (β-site APP cleavage enzyme 1) and γ-secretase activity is believed to be a key pathogenic event in AD (*6*). As a result, strategies that reduce BACE1 activity, and thereby Aβ levels, have been considered as a potential therapeutics for AD (*7*, *8*). A skin patch consisting of BACE1 inhibitor therapeutics has entered phase 3 clinical trial (*9*). However, several BACE1 small-molecule inhibitors have been shelved by pharmaceutical companies due to off-target toxicity and other safety reasons (*10*, *11*). Despite these recent failures, BACE1 is still considered as one of the most promising therapeutic targets for AD (*8*, *11*).

Compared to small molecule–based approaches, small interfering RNAs (siRNAs) offer promising therapeutics for brain disease treatment by directly blocking causative gene expression with high targeting specificity, low effective doses, and a relatively simple drug development process (*12*). siRNA in a lentiviral vector silencing BACE1 has also been shown to ameliorate AD neuropathology (*13*). However, effective and safe systemic delivery of siRNA into the brain remains challenging, reflecting the presence of biological barriers such as the blood-brain barrier (BBB), short circulation lifetime, enzymatic degradation, insufficient tissue penetration, cell endocytosis, and impaired cytosolic transport. Recent studies have shown that nanodelivery approaches hold great potential for overcoming these challenges (*12*). It has been reported that the delivery of BACE1 siRNA (siBACE1) to the mouse brain by systemic injection can partially reduce AD neuropathology (*14*, *15*). However, the therapeutic efficacy was less than ideal probably due to low siRNA brain accumulation and poor stability. In this work, we report an effective, nonviral, and BBB-penetrable siBACE1 nanodelivery approach that we evaluate in a well-established AD mice model that offers the potential for clinical translation.

We developed a glycosylated nanodelivery system, which uses glycemia-controlled Glut1 (glucose transporter-1) recycling to facilitate nanomedicine BBB penetration for more effective AD therapy (Fig. 1). To improve biophysiological protection of the encapsulated siRNA, we used a "triple-interaction" stabilization method reported previously (*16*). Specifically, we make use of a guanidinium-phosphate ($Gu^+/PO_3^{4-}$) salt bridge to provide a stabilizing electrostatic and hydrogen bond interaction, in addition to the hydrophobic interaction, which is derived by the complexation between siRNA and the galactose-modified poly(ethylene glycol)-*block*-poly[(*N*-(3-methacrylamidopropyl) guanidinium [Gal-PEG-*b*-P(Gu)]/poly(ethylene glycol)-*block*-poly [(*N*-(3-methacrylamidopropyl) guanidinium-*co*-2,2,3,3-tetrafluoropropyl

[1]State Key Laboratory of Medicinal Chemical Biology, College of Pharmacy, Nankai University, Tianjin 300350, China. [2]Henan-Macquarie Uni Joint Centre for Biomedical Innovation, School of Life Sciences, Henan University, Kaifeng, Henan 475004, China. [3]School of Pharmacy, Henan University, Kaifeng, Henan 475004, China. [4]Department of Bioengineering, Graduate School of Engineering, The University of Tokyo, 7-3-1 Hongo, Bunkyo-ku, Tokyo 113-8656, Japan. [5]Department of Biomedical Sciences, Faculty of Medicine & Health Sciences, Macquarie University, Sydney, NSW 2109, Australia. [6]Center for Nanomedicine and Department of Anesthesiology, Brigham and Women's Hospital, Harvard Medical School, Boston, MA 02115, USA. [7]Institute for Biomedical Materials & Devices (IBMD), School of Mathematical and Physical Sciences, University of Technology Sydney, 15 Broadway, Ultimo, NSW 2007, Australia. [8]Florey Institute of Neuroscience and Mental Health, University of Melbourne, Melbourne, VIC 3010, Australia.
*These authors contributed equally to this work.
†Corresponding author. Email: bs@henu.edu.cn (B.S.); xuexue@nankai.edu.cn (X.X.); mzheng@henu.edu.cn (M.Z.)

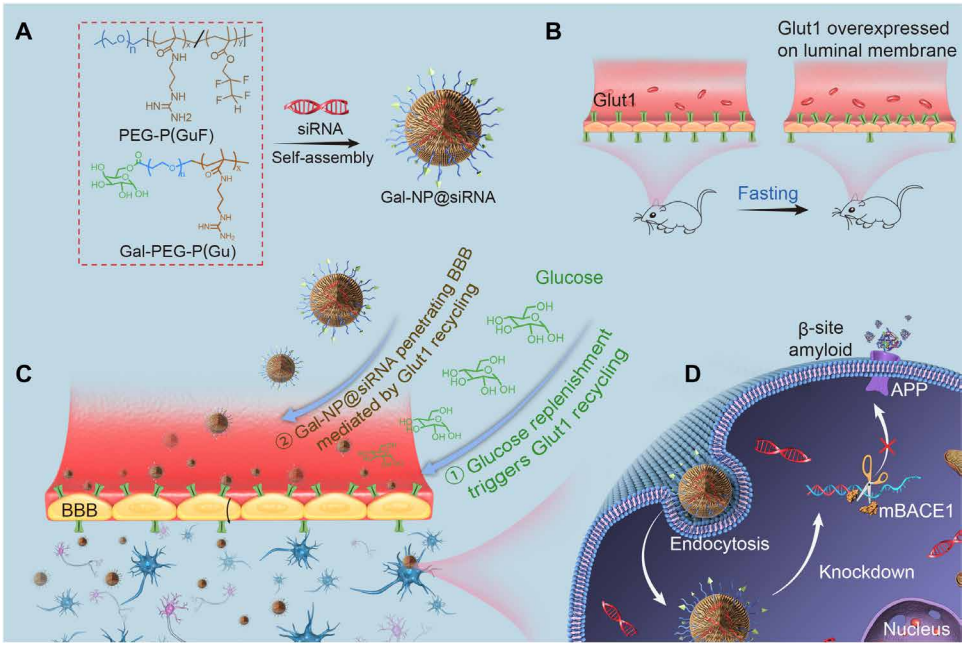


**Fig. 1. Illustration of the formation of the glycosylated "triple-interaction" stabilized siRNA nanomedicine (Gal-NP@siRNA) and the mechanism and approach to treat AD pathology in APP/PS1 transgenic mice.** (**A**) Schematic illustration of the fabrication of Gal-NP@siRNA. (**B** and **C**) Mechanism by which Gal-NP@siRNA penetrates the BBB and accumulates in the brain. Glut1 is overexpressed on the luminal membrane of the BBB after 24-hour fasting. After treatment with Gal-NP@siRNA, glucose replenishment in fasting mice results in Glut1 recycling from the luminal to the abluminal membrane of the BBB, which leads to the transport of Gal-NP@siRNA across the BBB. (**D**) Gal-NP@siRNA–mediated knockdown of BACE1 mRNA expression, which leads to reduced levels of amyloid plaques.

methacrylate] [PEG-*b*-P(GuF)] polymer mixture. Our triple-interaction stabilized siRNA nanomedicine demonstrates superior stability performance in blood circulation relative to conventional cationic polymer-based nanomedicines that feature only a single electrostatic interaction (*16*). Furthermore, exploiting Glut1 recycling by initially inducing hypoglycemia, which elevates Glut1 expression on the luminal plasma membrane of the BBB, facilitates markedly enhanced delivery of glucose-modified nanocarriers across the BBB when Glut1 is recycled to the abluminal membrane of the BBB upon glucose replenishment (*17*–*19*). To facilitate the Glut1 recycling approach, we appreciated that Glut1 stereochemistry allows binding of both D-glucose and D-galactose (*20*–*23*). We thus hypothesized that our galactose-modified siRNA nanomedicines should bind to Glut1 to efficiently penetrate the BBB by glycemia-controlled Glut1-mediated transport. Consequently, we demonstrate that siBACE1 glycosylated siRNA nanomedicine is efficiently delivered to the brains of APP/PS1 transgenic mice and ameliorates AD-like pathology, leading to improvement in cognitive impairment.

## RESULTS

### Biophysical characterization and in vitro studies of Gal-NP@siRNA

In this study, the glycosylated triple-interaction stabilized siRNA nanomedicine (Gal-NP@siRNA) was prepared by complexation between siRNA and Gal-PEG-*b*-P(Gu)/PEG-*b*-P(GuF), which were synthesized by reversible addition-fragmentation chain transfer copolymerization of hydrophobic monomer 2,2,3,3-tetrafluoropropyl methacrylate and siRNA complexation segment *N*-(3-methacrylamidopropyl) guanidinium (Gu) (for detailed synthesis, see scheme S1 and fig. S1). Because of the hydrophobic interaction of the fluorine in P(GuF) for nucleic acid stabilization enhancement (*16*, *24*), gel retardation assays demonstrated that the Gal-PEG-*b*-P(Gu)/PEG-*b*-P(GuF) polymer mixture can more effectively encapsulate siRNA compared to the fluorine-free Gal-PEG-*b*-P(Gu) polymers (complete siRNA loading weight ratio: 2.5:1 versus 10:1) (Fig. 2A and fig. S2A). Moreover, fluorinated nanomedicines showed better performance in stability assays compared to fluorine-free counterparts in the negatively charged biomacromolecule heparin competition assay (fig. S2B), signifying the importance of fluorination to improve the stability of siRNA nanomedicines. These siRNA nanoparticles (NPs) were then characterized by dynamic light scattering (DLS) and transmission electron microscopy (TEM) (Fig. 2, B and C). These results showed that Gal-NP@siRNA nanomedicine exhibited a spherical morphology with an average size of 118 nm and a low polydispersity index of 0.13 at a polymer/siRNA mass ratio of 2.5:1. Moreover, the nanomedicine exhibited excellent stability in both phosphate-buffered saline (PBS) and 10% fetal bovine serum (FBS) (fig. S2C).

A key point for siRNA nanodelivery for AD therapy is an effective neural cell endocytosis and cytosolic transport. Flow cytometry analysis and confocal imaging showed that both glycosylated and nonglycosylated siRNA nanomedicines are efficiently taken up by Neuro-2a cells (Fig. 2, D and E). The Gal-NP@siRNA nanomedicine also displayed effective endosome escape ability (fig. S3). In addition, competitive cellular binding assay of Gal-NP@Cy5-siRNA in general Glut1 inhibitor phloretin treatments showed a dose-dependent uptake in Glut1 highly expressed cells (fig. S4), which is consistent with previous report (*18*), indicating Glut1 as the dominant endocytosis pathway. Next, to quantify the efficiency of siRNA silencing of the target gene, BACE1 mRNA and protein expression were examined

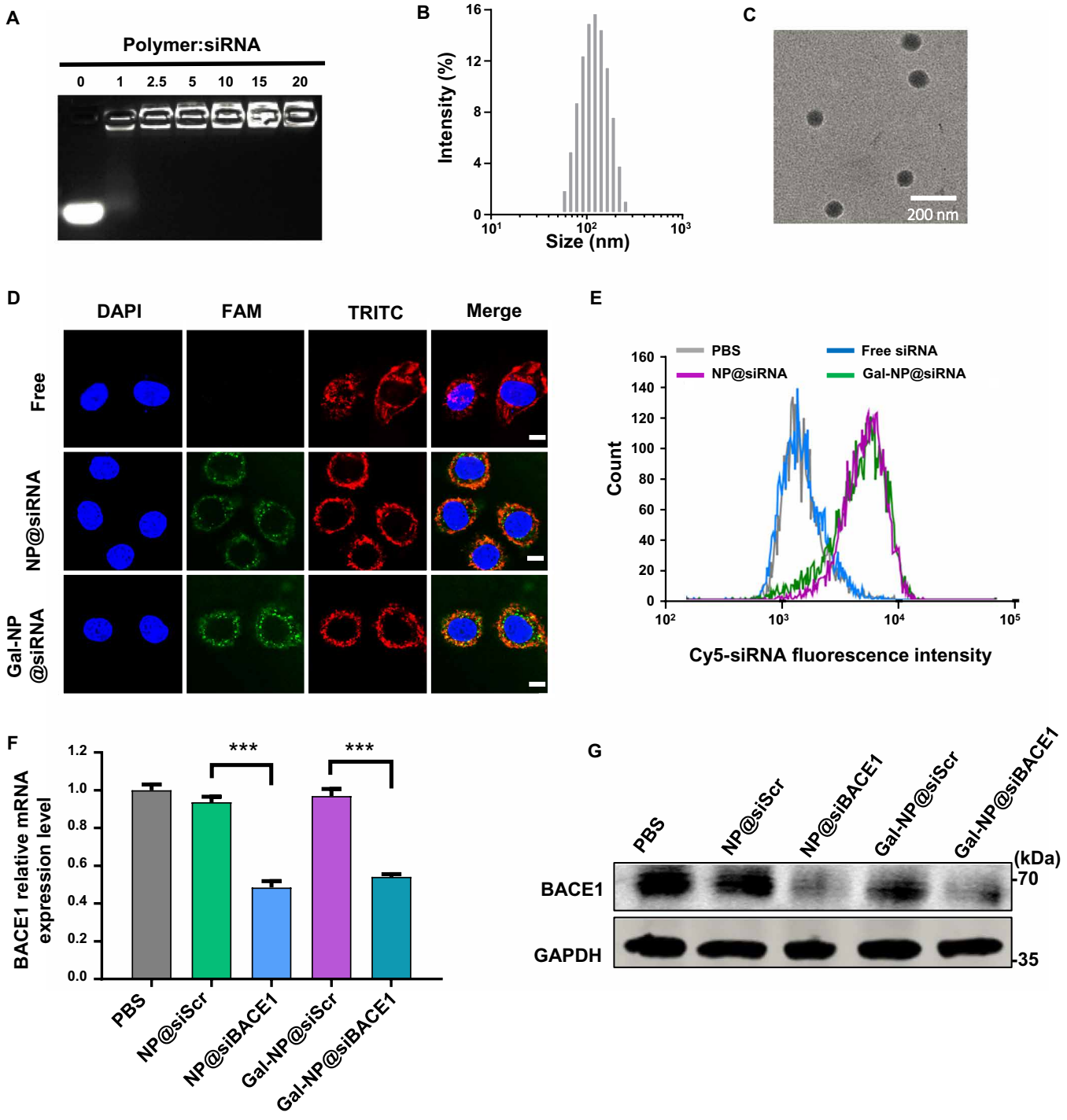


**Fig. 2. Biophysical characterization and in vitro studies of Gal-NP@siRNA.** (**A**) Gel retardation assay of Gal-NP@siRNA at polymer/siRNA weight ratios of 1, 2.5, 5, 10, 15, and 20. (**B**) Size distribution and (**C**) transmission electron micrographs of Gal-NP@siRNA. (**D**) Confocal laser scanning microscopy images for NP cellular uptake. Images were collected for Neuro-2a cells after 4-hour NP incubation. Cell nuclei were stained with DAPI (blue), siRNA was labeled by FAM dye (green), and cell cytoskeleton was stained with TRITC-phalloidin (red) to indicate cytoplasm area. Scale bars, 10 μm. (**E**) Flow cytometry analysis of Neuro-2a cells following 4-hour incubation with free Cy5-siRNA, NP@Cy5-siRNA, and Gal-NP@Cy5-siRNA. (**F** and **G**) In vitro gene silencing effects of Gal-NP@siBACE1 and controls at day 3 post transfection. BACE1 mRNA (F) and protein (G) expression levels was quantified by qRT-PCR and western blot assay, respectively. Data are presented as mean ± SEM ($n = 3$, $^{***}P < 0.001$).

in Neuro-2a cell samples treated with Gal-NP@siBACE1. The results showed that the BACE1 gene was sufficiently silenced in Neuro-2a cells (Fig. 2, F and G), achieving approximately 46 and 45% BACE1 mRNA and protein down-regulation, respectively, while exhibiting no obvious toxicity in multiple neuron-related cells (fig. S5). In contrast, NPs loaded with scrambled siRNA (siScr) failed to reduce BACE1 mRNA and protein levels, corroborating the sequence-specific gene silencing activity of siBACE1. The superior silencing

ability of Gal-NP@siBACE1 in Neuro-2a cells likely reflects their stable encapsulation and siRNA protection, efficient cellular internalization, and endosome escape, characteristics that show promising potential for in vivo study.

### Biodistribution and in vivo BACE1 targeting efficacy of Gal-NP@siRNA

Next, to evaluate in vivo pharmacokinetics, the plasma levels of Cy5-labeled siRNA were measured after intravenous injection of free siRNA, fluorinated siRNA nanomedicine, and fluorine-free siRNA nanomedicines. These data demonstrated that the fluorinated siRNA nanomedicine (Gal-NP@siRNA) had the longest blood circulation time with an elimination half-lifetime ($t_{1/2}$) of 39.2 min (Fig. 3A), which was significantly longer than that of both the fluorine-free counterpart and free siRNA ($t_{1/2}$ of 22.0 and 8.0 min, respectively; fig. S6A and Fig. 3A). These circulation results were consistent with the data above demonstrating biophysical stability and good heparin competition characteristics, further confirming the excellent stability of fluorinated siRNA NPs. Subsequently, we studied the in vivo brain targeting of our glycosylated siRNA nanomedicine by glycemia-controlled Glut1-mediated transport. The biodistribution of Gal-NP@Cy5-siRNA was quantified by fluorometry. These experiments demonstrated that the brain accumulation of Gal-NP@Cy5-siRNA nanomedicine was up to 5.8-fold higher than that of non–galactose-modified NP@Cy5-siRNA nanocarriers (Fig. 3B and fig. S6B). In addition, we also observed that the siRNA brain accumulation reached a peak at 1 hour after injection and maintained a considerable fluorescence accumulation up to 24 hours, as monitored by Cy5 in vivo imaging (Fig. 3C), and the BACE1 mRNA and protein expression in cortex was inhibited after nanomedicine treatment (Fig. 3, D and E, and fig. S6C).

### Behavioral evaluation of Gal-NP@siBACE1 nanomedicine therapy in APP/PS1 mice

To evaluate the therapeutic effect of Gal-NP@siBACE1 in a relevant AD pathology model, the APP/PS1 double transgenic mouse model was assessed in behavioral tests of learning and memory impairment relevant to AD. The APP/PS1 double transgenic mouse is a commonly used multitransgenic animal model that expresses two familial AD mutant genes for APP together with mutant presenilin 1 (PS1). Compared to single transgenic mice and other nongenetic AD mouse models, APP/PS1 mice express accelerated amyloid deposition and synaptic loss with reliable memory deficits (*25*–*27*). BACE1 inhibition has been reported to prevent neuron loss and memory deficits in APP/PS1 mice (*28*), demonstrating suitability for evaluating the therapeutic efficacy of novel nanocarriers in this model.

To determine whether Gal-NP@siBACE1 nanomedicine could ameliorate neuropathology in APP/PS1 transgenic mice, APP/PS1 mice were given Gal-NP@siBACE1 or control Gal-NP@siScr (siRNA, 1 mg/kg) via caudal vein injection every 3 days (Fig. 4A). The same dose of non–galactose-modified NP@siBACE1 was assessed as a negative control. PBS-injected APP/PS1 and control wild-type (WT) mice groups were included to ascertain AD-relevant deficits in APP/PS1 mice at baseline. Behavioral tests including the novel object recognition (NOR) test and the Morris water maze (MWM) were performed to examine spatial learning and memory, while the nest-building test was used to assess general health and hippocampal function, because nest building is often impaired in rodent models of AD (*29*–*32*).

Experimental nesting data showed that Gal-NP@siBACE1–treated APP/PS1 mice achieved a similar score to WT mice, which was much better than all other APP/PS1 control groups (Fig. 4, B and C). Furthermore, the NOR test results showed that PBS-treated APP/PS1 control mice showed suppressed interest in exploring novel objects compared with WT mice as determined by discrimination index (DI) and preference index (PI) for novel object (Fig. 4, D to F). After being treated with Gal-NP@siBACE1, APP/PS1 mice showed a significant increase in NOR compared to PBS-treated APP/PS1 control mice. Excitingly, the DI and PI for novel object reached the performance of normal WT mice (Fig. 4, E and F). In contrast, control APP/PS1 mice treated with non–galactose-modified NP@siBACE1 or Gal-NP@siScr performed as poorly as PBS-treated control APP/PS1 mice, signifying the importance of the targeting ability of the galactose ligand and the therapeutic effect of siBACE1 brain delivery. In the MWM test, all groups achieved comparable escape latencies (fig. S7) during the five training days.

On the probe test day, when the escape platform was removed, long-term spatial memory has been investigated (Fig. 4, G to J). However, on probe test day, mice administered with PBS, NP@siBACE1, and Gal-NP@siScr showed an aimless searching strategy with no or only slightly improved spatial learning and memory (see representative tracking plots in Fig. 4G), with reduced time in the target quadrant but similar swimming speed compared to WT controls (Fig. 4, H and I). In contrast, APP/PS1 mice treated with Gal-NP@siBACE1 exhibited a greater proportion of time in the target quadrant and number of platform crossings compared to PBS-injected controls (Fig. 4, I and J). These data confirm that the Gal-NP@siBACE1 nanomedicine mediates highly effective siRNA brain delivery to significantly improve cognitive performance in APP/PS1 mice.

### Effects of the Gal-NP@siBACE1 treatment on APP processing and amyloid deposition in APP/PS1 mice

After behavioral tests were completed, mice were sacrificed, and brain tissue was collected for analysis of BACE1 suppression and its impact on Aβ and tau pathological accumulation (Fig. 5A). Our results showed that both hippocampal and cortical BACE1 protein levels in Gal-NP@siBACE1–treated APP/PS1 mice were significantly decreased compared to other APP/PS1 control groups (Fig. 5B and fig. S8, A and B), in agreement with the improvement in behavioral tests. Hence, effective BACE1 protein silencing shown by Gal-NP@siBACE1 demonstrates a reliable siRNA delivery approach for targeting the brain. The manifestation of pathological hallmark of AD, amyloid plaques derived from BACE1-cleaved APP, was significantly decreased with reduced foci size in both the hippocampus and cortex of Gal-NP@siBACE1–treated APP/PS1 mice (Fig. 5, C and D). In sharp contrast, control PBS–, NP@siBACE1-, or Gal-NP@siScr–treated mice exhibited pronounced Aβ plaque deposition (Fig. 5, C and D). Another major pathological feature of late-stage AD is the development of intracellular neurofibrillary tangles composed of hyperphosphorylated tau protein (p-tau), which synergistically impairs cognitive performance in AD patients (*33*). Our data showed that both hippocampal and cortical p-tau levels in AD mice treated with Gal-NP@siBACE1 were lower than those in control AD mice treated with PBS (Fig. 5E and fig. S8C), probably attributable to the molecular interplay between Aβ and p-tau (*34*, *35*).

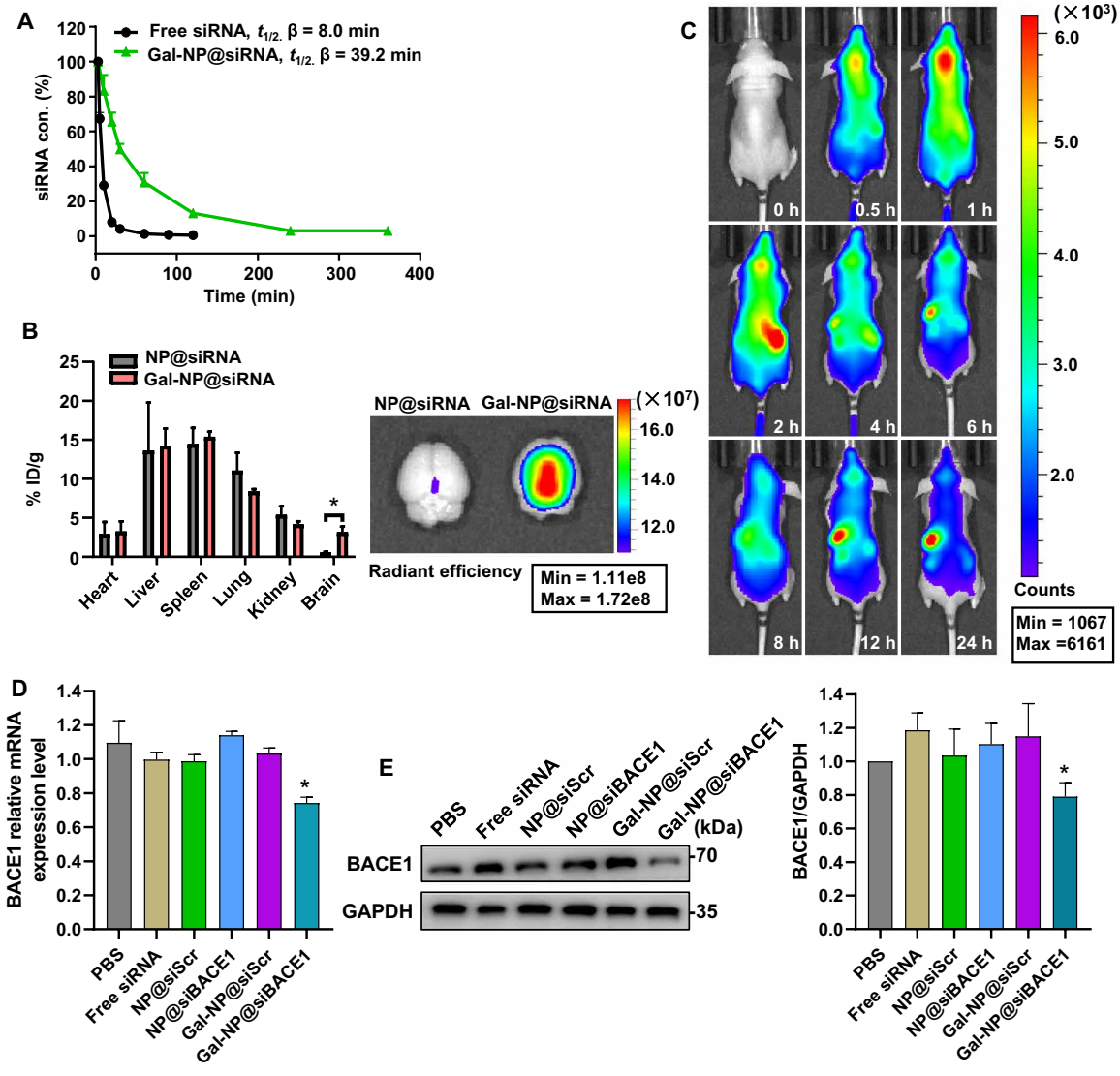


**Fig. 3. Biodistribution and in vivo BACE1 targeting efficacy of Gal-NP@siRNA.** (**A**) In vivo pharmacokinetics as shown by Cy5-siRNA concentration/time curves in plasma after a single-dose injection. (**B**) (Left) Quantification of Cy5-siRNA accumulation in different organs. Cy5-siRNA levels were determined by fluorescence spectroscopy 1 hour after tail vein injection of siRNA nanomedicine after a single-dose injection. Data are presented as mean ± SEM ($n = 3$, $^*P < 0.05$). (Right) Representative image for Cy5 signal in the brain of NP@siRNA and Gal-NP@siRNA groups 1 hour after injection. (**C**) Time course in vivo imaging of Gal-NP@Cy5-siRNA evaluated by fluorescence imaging after a single-dose injection. (**D** and **E**) BACE1 mRNA and protein expression level in cortex was quantified by (D) qRT-PCR and (E) Western blot assay from WT mice samples, and samples were collected at day 3 after two nanomedicine treatments. Data are presented as mean ± SEM ($n = 3$, $^*P < 0.05$).

BACE1 deficiency can impair remyelination, which negatively affects cognitive function (*36*). Therefore, it is imperative to knock down BACE1 to an appropriate therapeutic level. To check this, we followed the expression of the multilamellar myelin sheath formation marker myelin basic protein (MBP) in the central nervous system (CNS). In PBS-treated control APP/PS1 mice, the expression of MBP in the brain was significantly decreased (Fig. 5F and fig. S8D), indicating the negative consequences of Aβ deposition on myelin, which was consistent with reported literature (*37*). In contrast, MBP protein expression was restored in AD mice treated with Gal-NP@siBACE1 to levels seen in WT mice (Fig. 5F), thereby indicating that the dose of siBACE1 was appropriate and sufficient to neutralize Aβ toxicity.

## Cytotoxicity and in vivo biocompatibility assessment of the Gal-NP@siRNA nanomedicine

To further assess the biocompatibility and systemic response to the nanomedicine, we assessed routine blood parameters and chemistry by measuring plasma alanine aminotransferase (ALT), aspartate aminotransferase (AST), alkaline phosphatase (ALP), plasma urea (BUN), uric acid (UA), creatinine (CR), as well as blood platelet (PLT), red blood cells (RBCs), and white blood cells (WBCs) (Fig. 6, A and B, and fig. S9A). To evaluate the inflammatory concern of the nanomedicine treatments, core proinflammatory cytokines such as *Il-1*β, *Il-6*, and *Tnf*-α have been tested in liver and kidney (Fig. 6, C and D). These examinations demonstrated no significant difference between PBS and Gal-NP@siRNA treatment groups

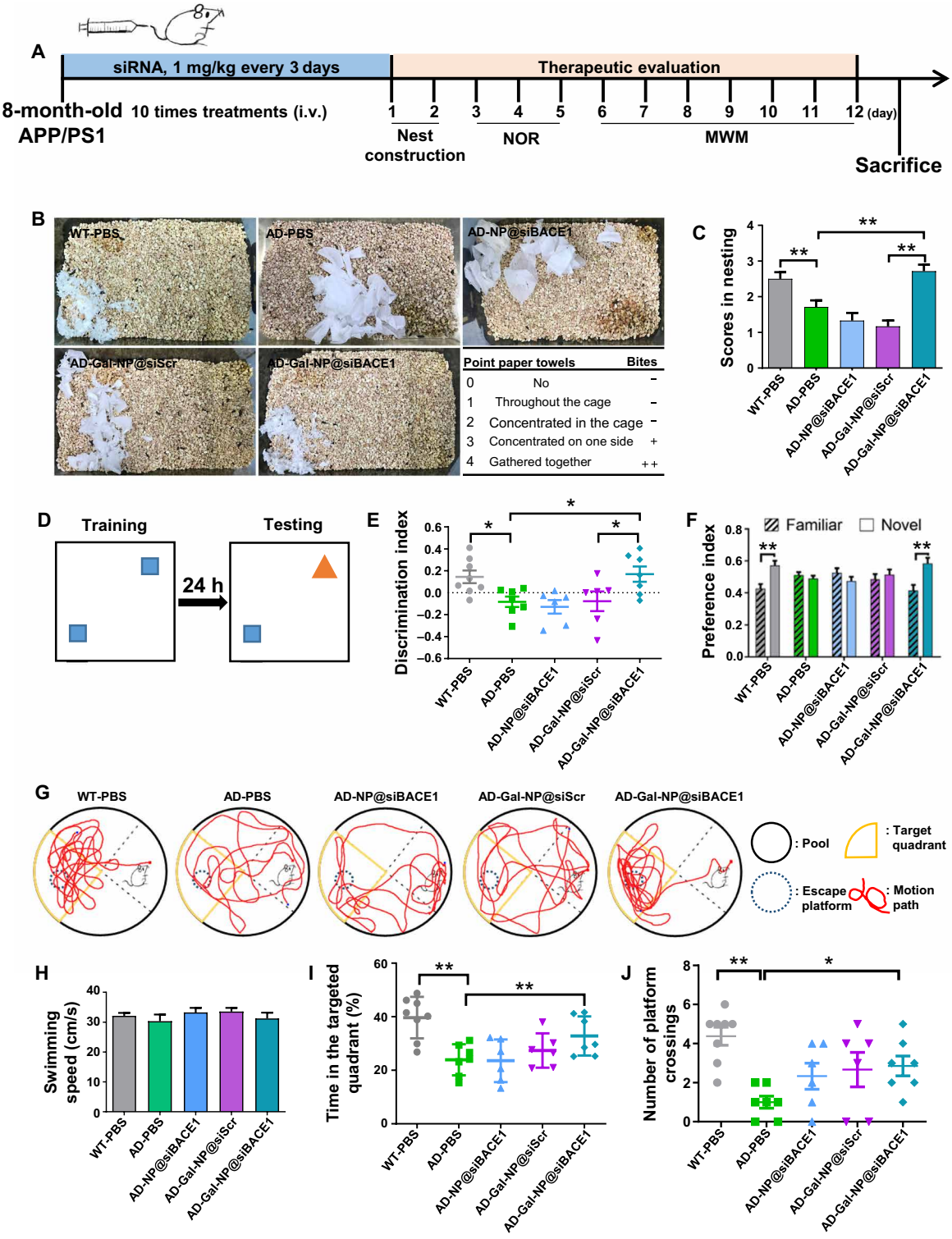


**Fig. 4. Behavioral evaluation of Gal-NP@siBACE1 nanomedicine therapy in APP/PS1 mice.** (**A**) Schematic of the experimental timeline. APP/PS1 and WT mice were treated with siRNA nanomedicine or PBS via tail vein injection every 3 days (10 cycles). Mice were then subjected to nesting, NOR, and MWM tests for memory evaluation, and samples for molecular pathological assessments were collected. (**B**) Representative images and scoring criteria from the nest-building experiment in APP/PS1 and control WT mice. Photos were taken 24 hours after the introduction of nesting material to the home cage. Photo credits: Yutong Zhou, Nankai University. (**C**) Nest-building scores for each group. (**D**) Setup for NOR test. (**E** and **F**) Results for NOR test. (E) DI and (F) PI of each group after nanomedicine treatment. (**G** to **J**) Data for probe test in the MWM. (G) Representative swimming track, (H) swimming speed, (I) ratio of time spent in target quadrant, and (J) number of crossing the platform location of each group on the probe test day. All behavioral test bar or plot charts are presented as mean ± SEM ($n = 6$ to 8, $^{*}P < 0.05$, $^{**}P < 0.01$).

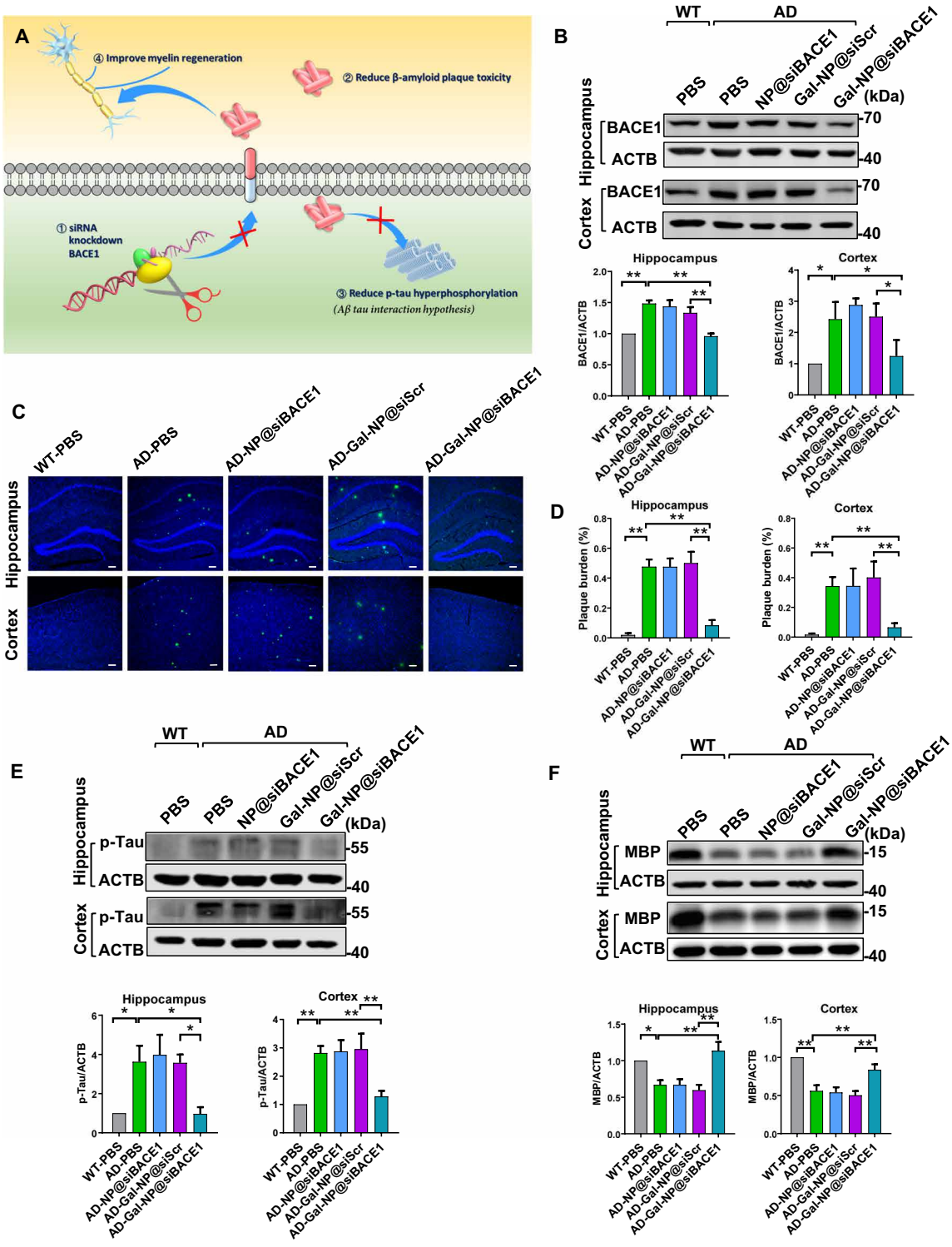


**Fig. 5. Therapeutic evaluation of the ability of Gal-NP@siBACE1 treatment to modulate AD hallmarks in APP/PS1 mice.** (**A**) Mechanistic explanation for the effects of siBACE1 therapy. (**B**) Representative Western blot data for BACE1 protein expression in hippocampus and cortex from nanocarrier-treated APP/PS1 mice, control APP/PS1 groups, and WT mice. Quantification of Western blotting analysis of BACE1 expression was relative to β-actin ($n = 3$, mean with SEM, $^{*}P < 0.05$, $^{**}P < 0.01$). (**C**) Representative confocal laser scanning microscopy imaging data assessing amyloid plaque burden. Immunofluorescence of Aβ plaques (green) in hippocampus and cortex from APP/PS1 transgenic and WT mice. Nuclei were stained by DAPI (blue). Scale bars, 100 μm. (**D**) Percent surface area of amyloid plaques in hippocampus (left) and cortex (right) regions was quantified. Data are presented as mean ± SEM; $n = 4$, $^{**}P < 0.01$. (**E**) p-tau and (**F**) MBP expression in the hippocampus and cortex for nanocarrier-treated APP/PS1 mice, control APP/PS1 groups, and WT mice (top). Quantification of Western blotting analysis was relative to β-actin (bottom) ($n = 3$, mean with SEM, $^{*}P < 0.05$, $^{**}P < 0.01$). All samples were collected after 10 administrations of nanomedicine.

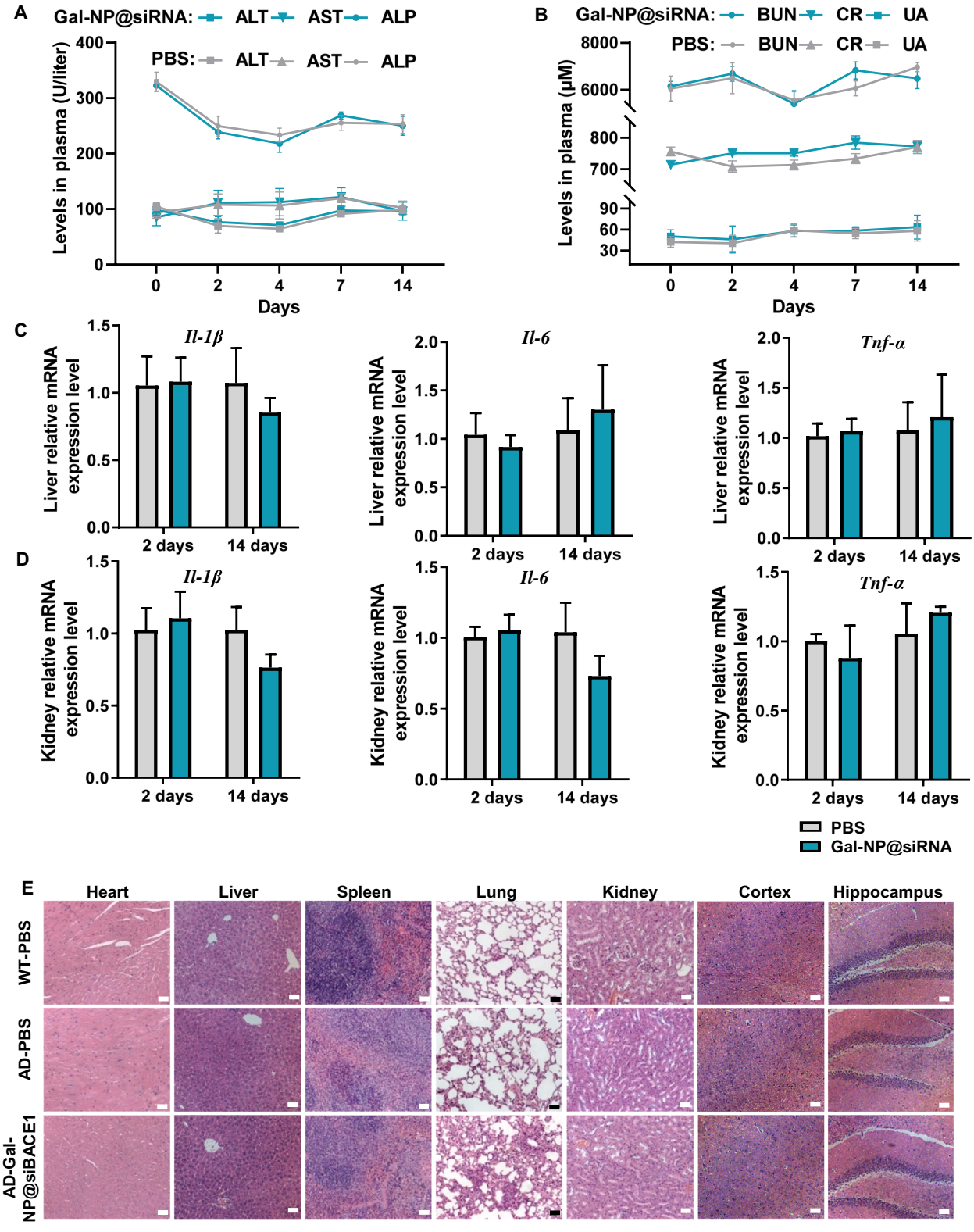


**Fig. 6. Cytotoxicity and in vivo biocompatibility assessment of the Gal-NP@siRNA nanomedicine.** (**A** and **B**) Blood chemistry examinations. Assessment of plasma alanine aminotransferase (ALT), aspartate aminotransferase (AST), alkaline phosphatase (ALP), plasma urea (BUN), creatinine (CR), and uric acid (UA) levels after a single-dose nanomedicine treatment. $n = 4$, mean with SEM. (**C** and **D**) Core proinflammatory cytokines such as *Il-1*β, *Il-6*, and *Tnf-*α in liver (C) and kidney (D) were assessed after a single-dose PBS or Gal-NP@siRNA nanomedicine treatment at days 2 and 14. $n = 3$, mean with SEM. (**E**) Representative data for hematoxylin and eosin staining in major organs from APP/PS1 and control WT mice treated with Gal-NP@siBACE1 or PBS in the 10-time injection therapeutic experiments. Scale bars, 50 μm.

within 2 weeks after injection, indicating that the Gal-NP@siRNA nanomedicine has a suitable safety profile and can survive free circulation in blood before its arrival at the target site in the brain. In addition, during nanomedicine therapy, there were no differences between treatment groups in body weight change or food uptake, further indicating the safety of the glycemia-controlled strategy for Gal-NP@siBACE1 nanocarriers (fig. S9B). Histochemical staining showed that treatment with Gal-NP@siBACE1 nanocarriers induced no necrosis or apoptosis in major organs (Fig. 6E) after 10 cycles of nanomedicine treatment.

## DISCUSSION

Integration of RNAi together with nanotechnology holds great promise for AD therapy. However, nanotechnology-based therapy has been put off by stringent regulatory framework (*12*, *38*). Clinical translation of nanomedicines is often hindered by multiple factors, including physical and chemical stability of nanomedicine, pharmacokinetic parameters, in vivo release mechanism, the robustness of manufacturing, route of administration, bioavailability, distribution, biodegradation, safety, accumulation, and appropriate animal studies (*39*, *40*). Most published studies examining nanomedicines as potential AD therapeutics address a limited number of these factors, which probably explains why these have largely been unsatisfactory in terms of efficacy and efficiency. In the work of Singer *et al.* (*13*), a siBACE1 lentiviral vector was applied by intracerebral injections. This early proof-of-concept study showed considerable potential in BACE1 silencing strategy. However, several critical limitations including toxicity, immunogenicity, and inflammatory response hinder the therapeutic use of the lentiviral vector in CNS disease (*41*). Also, intracerebral injection of the siRNA is destructive and may cause multiple side effects. Exosomes hold excellent capacity for reduce immunogenicity and siBACE1 brain delivery (*14*). However, preparing enough quantity of purified exosomes remains challenging when this concept moves to clinics. Polymeric NPs are easier to synthesize and scale up and also display low immunogenicity. A pioneering study developed synthesized polymeric nanoplatforms that deliver siRNAs to AD mice brain, but poor in vivo stability and ineffective brain accumulation limit its therapeutic effect (*15*). Still, more powerful nanomaterials are urgently needed to overcome current poor blood stability and inefficient BBB penetration (*42*). Here, we developed a self-assembly method based on galactose-decorated triple-interaction stabilized polymeric siRNA nanomedicine (Gal-NP@siRNA). Our nanomedicine formulation produces siRNA-loaded NPs through simple mixing of prepared polymers with the required siRNA sequence in a tunable ratio manner. The simplicity and versatility of our nanomedicine formulation can support assembly of NPs loaded with any short nucleic acids. We demonstrate that our nanomedicine formulation has superior physiological stability and blood longevity that is critical for siRNA to achieve high accumulation at diseased sites. To date, most reported siRNA nanomedicines were solely electrostatically stabilized, which makes them susceptible to dissociation in vivo, leading to short circulation time in blood. In this study, the combination of $Gu^{+}/PO_3^{4-}$ salt bridge that promotes additional electrostatic and hydrogen bond interaction with the fluorine-mediated hydrophobic interaction overcomes the stabilization problem of typical siRNA nanomedicines and further endows Gal-NP@siRNA with superior physiological stability and prolonged blood circulation time.

In addition to the stability challenge, effective BBB penetration is another big challenge for nanotechnology-based brain disease therapies. By design, our Gal-NP@siRNA–incorporated D-galactose makes it possible to exploit glycemic Glut1 recycling, enhancing the delivery of Gal-NP@siRNA across the BBB upon glucose administration. Potentially, this BBB-penetrating strategy is feasible clinically, as blood glucose spikes are easily induced through oral (glucose drink) or intravenous administration. Glut1 transporter expression and nutrition uptake decrease with age in AD patients (*43*, *44*). From this aspect, it may have an impact on the therapeutic efficiency of Gal-NP@siRNA to some extent, especially in a senior AD model. Another controversial point is that researchers found that BBB permeability increased in AD, which contributes to cognitive decline independently of AD pathology (*45*, *46*). However, the ineffective AD therapeutic ability of nontargeted NP@siRNA signifies the importance of Glut1-mediated transport for galactose-modified nanomedicines crossing the BBB.

In addition to excellent blood stability and effective BBB penetration, we also show that Gal-NP@siRNA nanomedicine exerts high brain accumulation. Gal-NP@siBACE1 decreased BACE1 expression, leading to reduced levels of Aβ plaques with the added benefit of suppressed phosphorylated tau protein levels and regeneration of impaired myelin. These positive pathophysiological effects probably contributed to the restoration of cognitive performance of Gal-NP@siBACE1–treated transgenic mice. In addition, Gal-NP@siRNA also exhibited excellent biocompatibility and did not cause renal or hepatic responses or adverse effects on myelination, suggesting that there is an effective clearance of by-products from the brain most likely via the paravascular glymphatic pathway (*47*).

AD is a complex neurodegenerative disorder, and the pathological pathways that govern AD are still controversial. Nonetheless, the toxic Aβ accumulation and tauopathy are two of the most reliable pathologic events in AD progression. In several early studies, inhibition of BACE1 mRNA levels lowers β-secretase activity associated with BACE1 and consequently reduces production of APPs and other proteins in cells (*48*–*50*). Therefore, BACE1 is considered one of the top drug targets for lowering cerebral Aβ plaque levels in AD.

We demonstrated partial knockdown of BACE1 protein expression, but there are several variants of that protein, and in subsequent studies, our Gal-NP@siRNA could be applied to carry multiple siRNAs for holistic therapy. In addition, our therapeutic approach is suitable for "gene therapy cocktail" applications.

In summary, we developed an effective strategy to deliver siBACE1 through the BBB with good circulation stability, which ameliorated AD-like pathology in APP/PS1 transgenic mice. These results indicate that our Gal-NP@siRNA nanomedicine has good clinical translation potential for AD therapy owing to ease of formulation, stability, and BBB penetration. Furthermore, our Gal-NPs could also be used to deliver siRNA in a wide range of CNS disease therapy including other neurodegenerative conditions and brain cancer.

## MATERIALS AND METHODS

### Materials

See the Supplementary Materials for the synthesis of MeO-PEG-*b*-P(GuF) and Gal-PEG-*b*-P(Gu). Primary antibody BACE1 (Abcam, AB183612), p-tau (Abcam, AB151559), MBP (Abcam, AB40390), β-actin (Abcam, AB8226), or glyceraldehyde-3-phosphate dehydrogenase (GAPDH) (Abcam, AB181602) and mouse or rabbit secondary

antibody (LI-COR IRDye 800CW) were used. All siRNAs were synthesized by GenePharma Company, and the sequences used were as follows: (i) Scramble: 5′-UUCUCCGAACGUGUCACGUdTdT-3′ (sense) and 5′-ACGUGACACGUUCGGAGAAdTdT-3′ (antisense); (ii) BACE1: 5′-GAACCUAUGCGAUGCGAAUdTdT-3′ (sense) and 5′-AUUCGCAUCGCAUAGGUUCdTdT-3′ (antisense). The siBACE1 sequence was shown in a previous work, which showed a better silencing effect among several sequences (*51*). A dye was introduced to the 5′-end of the antisense strand of siScr. For quantitative polymerase chain reaction (qPCR), all of these primers are designed by Primer-BLAST (National Center for Biotechnology Information) and listed in table S1.

### Nanocarrier characterization

$^1$H nuclear magnetic resonance spectra were recorded on AVANCE III HD 400 MHz (Bruker, Switzerland). The size was determined at 25°C using DLS (Zetasizer Nano-ZS, Malvern Instruments) equipped with a 633-nm He-Ne laser using backscattering detection. TEM was performed using a JEM-2100 TEM operated at an accelerating voltage of 200 kV (JEOL, Japan). The confocal laser scanning microscopy images of cells were taken on a Zeiss Confocal Microscope system (Zeiss 880). The transfected cells were observed with a microplate reader (Molecular Devices, USA), and fluorescence was quantitatively measured by flow cytometry (BD FACSCalibur, San Jose). The gel electrophoresis images were taken by Molecular Imager FX (Bio-Rad, Hercules, CA). The fluorescent images were scanned using a near-infrared fluorescence imaging system (Lumina, IVIS III).

### Gel retardation assay

siRNA (0.5 mg) was dissolved in 500 μl of diethyl pyrocarbonate–treated water. Polymer and siRNA solutions were mixed (the amount of siRNA was 2 μM) at polymer/siRNA weight ratios of 1:1, 2.5:1, 5:1, 10:1, 15:1, and 20:1. The mixture was incubated for 30 min. The siRNA binding ability of polymer was studied by agarose gel. The polymer/siRNA ratios were electrophoresed through a 2% agarose gel containing Gel Red at 35 V in TAE solution [40 mM tris-HCl, 1% acetic acid (v/v), and 1 mM EDTA]. Fluorine-free Gal-NP (mixed with siRNA at a mass ratio of 10:1) and fluorinated Gal-NP (mixed with siRNA at a mass ratio of 2.5:1) were prepared, and then different doses of heparin solution were added to the NPs. siRNA release was measured by a nucleic acid gel at different time points.

### siRNA nanomedicine formulation

The siRNAs were dissolved in Hepes buffer (pH 7.4) to a stock concentration of 4000 nM (53.2 μg/ml) for in vitro experiments and 400 μg/ml for animal experiments. The polymer solution was added into the siRNA solution (volume ratio = 1:1) and then gently pipetted 10 times and incubated for 30 min at room temperature. Then, the prepared nanomedicines were diluted into a working concentration of 200 or 400 nM siRNA for in vitro experiments and 200 μg/ml for in vivo experiments. Gal-PEG-b-P(Gu) and MeO-PEG-b-P(Gu)/MeO-PEG-b-P(GuF) (molar ratio = 1:3) complexed with siRNA yielded nanomedicine denoted as fluorine-free Gal-NP@siRNA (polymer/siRNA weight ratio = 10) and NP@siRNA (polymer/siRNA weight ratio = 2.5:1). Gal-PEG-b-P(Gu)/MeO-PEG-b-P(GuF) (molar ratio = 1:3) complexed with siRNA yielded Gal-NP@siRNA nanomedicine (polymer/siRNA weight ratio = 2.5:1).

### Flow cytometry assay

Neuro-2a cells were seeded in a six-well plate ($1 \times 10^6$ cells per well) and incubated with PBS, Gal-NP@Cy5 siRNA, NP@Cy5-siRNA, and naked Cy5-siRNA in 500-μl medium (200 nM Cy5-siRNA) at 37°C for 4 hours. The cells were digested by 0.25% (w/v) trypsin and 0.03% (w/v) EDTA. The suspensions were centrifuged at 1000 rpm for 3 min, washed twice with PBS, and then resuspended in 500 μl of PBS. Fluorescence histograms were immediately recorded with a BD FACSCalibur flow cytometer (Becton Dickinson, USA) and analyzed using CellQuest software based on 10,000 gated events. The gate was arbitrarily set for the detection of Cy5 fluorescence.

### In vitro cytotoxicity assay

Neuro-2a, SH-SY5Y, and PC-12 cells were seeded in 96-well plates (6000 cells per well) and incubated in 100 μl of culture medium for 24 hours. Thereafter, PBS, NP@siRNA, Gal-NP@siRNA, and naked siRNA NPs were added to the cells, and the cells were then incubated for 48 hours. At assay end, 3-(4,5)-dimethylthiahiazo (-z-y1)-3,5-diphenytetrazoliumromide (MTT) solution (5 mg/ml, 1 μl/10 μl of medium) was added and samples were further incubated at 37°C for 4 hours. Cell viability was determined from the absorbance of extracellular medium at 570 nm.

### Gene silencing assay by quantitative real-time PCR

Endogenous BACE1 gene silencing activity of Gal-NP@siRNA was investigated by quantitative real-time PCR (qRT-PCR). Neuro-2a cells were seeded in a six-well plate ($1 \times 10^6$ cells per well) in growth medium (Minimum Essential Medium/Earle's Balanced Salt Solution also known for MEM/EBSS containing 10% FBS) for 24 hours. The medium was removed and replenished with fresh medium (1000 μl) containing PBS, NP@siScr, NP@siBACE1, Gal-NP@siScr, and Gal-NP@siBACE1 (400 nM siRNA). After 3 days, the cells were washed with PBS and the total RNA was extracted using the RNeasy Mini Kit (Qiagen).

For mice experiments, normal female Balb/c mice were randomly divided into two treatment groups ($n = 3$). PBS and Gal-NP@siScr (1 mg of siRNA equiv./kg) were intravenously injected into mice via the tail vein ($n = 3$ per group). At prescribed time points after injection, animals were anesthetized and transcardially perfused with saline. The tissues were homogenized in 1 ml of ice-cold TRIzol reagent (Invitrogen) according to the protocol of the manufacturer. Reverse transcription and qPCR were carried out by following reverse transcription protocol (Takara) and SYBR Green Gene Expression Assays Protocol (Takara) with the Roche LightCycler 480 RT-PCR System. mGAPDH was used as an endogenous housekeeping gene to normalize the Bace1 mRNA. The mRNA expression level was calculated based on comparative $C_t$ method ($2^{-\Delta\Delta Ct}$).

### Animals

All animals used for experiments were allocated blindly to treatment groups. All protocols were approved by the Animal Care and Use Committee of Laboratory Animal Center, Henan University (ethics approval number: HUSOM-2018-354). Adult, 8-week female Balb/c mice were used in the biodistribution assay, in vivo BACE1 silencing, and blood biochemistry examinations. For in vivo imaging experiments, 8-week female nude mice were used. For therapeutic evaluation experiments and animal behavior tests, 8-month male APP/PS1 and C57BL/6 mice (WT-like littermates) were used. All mice were provided by Beijing Vital River Laboratory Animal

Technology Co. Ltd. and transported to the animal facility at Nankai University or Henan University at least 2 weeks before testing. Mice were housed in a standard individual ventilation cages animal experimental system (Suzhou Fengshi Laboratory Animal Equipment Co. Ltd.) with corn cob bedding and a wire lid, providing climbing opportunities (APP/PS1 and its control mice were housed one mouse per cage for experiments). Mice were kept under a 12:12-hour day-night schedule; food and water were available ad libitum. Separate cohorts were used for each experiment ($n$ = 6 to 8 per treatment group, WT-PBS = 8, AD-PBS = 7, AD-NP@siBACE1 = 6, AD-Gal-NP@siScr = 6, AD-Gal-NP@siBACE1 = 7). Food was removed for fasting 24 hours before nanomedicine treatment. Two hundred microliters of 20 weight % (wt %) glucose was administered to all groups by intraperitoneal injection 30 min before nanomedicine injection. For nanomedicine treatment, we administered NPs modified with or without galactose (Gal-NP@siBACE1 or NP@siBACE1) to verify Glut1 targeting and effective brain delivery. Gal-NPs loaded with siBACE1 or siScr (Gal-NP@siBACE1 or Gal-NP@siScr) were designed to assess gene silencing efficiency. APP/PS1 and WT-like mice injected with 200 μl of PBS were used as controls to demonstrate pathological dysfunction in AD mice. All AD nanomedicine therapy groups were given 1 mg of siRNA equiv./kg diluted in 200 μl of PBS via caudal vein injection every 3 days. Treatment schedules for injection of siRNA nanomedicines and behavior test date are highlighted in Fig. 4A.

### Pharmacokinetics

Gal-NP@Cy5-siRNA, fluorine-free Gal-NP@Cy5-siRNA, and naked Cy5-siRNA (1 mg of Cy5-siRNA equiv./kg) in 200 μl of Hepes were intravenously injected into mice via the tail vein ($n$ = 3). At prescribed time points after injection, ~50 μl of blood was taken out from the eye socket of mice. The blood samples were immediately dissolved in 0.6 ml of lysis buffer (1% Triton X-100) at 37°C overnight followed by centrifugation (14,000 rpm, 30 min). The Cy5 level in the supernatant was determined by fluorometry. The blood circulation followed a typical two-compartment model: a rapid decline in the distribution phase and a long period in the elimination phase. We calculated the half-lives of two phases ($t_{1/2,\alpha}$ and $t_{1/2,\beta}$) by fitting the experimental data using SoftwareS6 Origin 8 exponential decay 2 model: $y = A_1 \times \exp(-x/t_1) + A_2 \times \exp(-x/t_2) + y_0$, and then taking $t_{1/2,\alpha} = 0.693 \times t_1$ and $t_{1/2,\beta} = 0.693 \times t_2$.

### Biodistribution

After fasting (1 day), glucose solution (20 wt %) was injected to elevate the blood glucose concentration, and 30 min later, a single dose of NP@Cy5-siRNA and Gal-NP@Cy5-siRNA in 200 μl of Hepes was administrated intravenously via the tail vein (1 mg of siRNA equiv./kg). After 1 hour, the mice were sacrificed. The major organs including heart, liver, spleen, lung, kidney, and brain were collected, washed, dried, weighed, and homogenized in 0.6 ml of 1% Triton X-100 with a homogenizer at 14,000 rpm for 30 min. Cy5 in the supernatant was determined by fluorometry based on a calibration curve and expressed as injected dose per gram of tissue (%ID/g).

### In vivo and ex vivo imaging

To evaluate the in vivo brain targeting ability of NPs, Gal-NP@Cy5-siRNA and NP@Cy5-siRNA were injected intravenously to nude mice and monitored at different time points by using the Lumina IVIS III Imaging System (excitation = 620 nm; emission = 670 nm).

To evaluate the ex vivo brain targeting and NP biodistribution, Gal-NP@Cy5-siRNA and NP@Cy5-siRNA were injected intravenously to nude mice after fasting. One hour after injection, main organs were separated, washed in PBS, and monitored.

### Western blot

Neuro-2a cells were harvested at day 3 after incubation with Gal-NP@Cy5-siRNA and control vectors. For sufficient siBACE1 verification, mouse brain tissues were taken from Balb/c mice after two siRNA injections. In therapeutic evaluation, mouse brain tissues were taken 1 day after completion of behavioral assessments. Animals were anesthetized and transcardially perfused with saline. Tissue (whole hippocampus and cortex) and cells were homogenized in radioimmunoprecipitation assay lysis buffer with a proteinase and phosphorylase inhibitor cocktail (Thermo Fisher Scientific) and centrifuged for 15 min (12,000 rpm, 4°C). The protein concentration of the supernatant was determined using the BCA Protein Assay Kit (Beyotime, China). Standard Western blot electrophoresis was then performed, with proteins transferred onto polyvinylidene difluoride membranes (Millipore 0.22 μm) and immunoblotted. Primary antibody BACE1 (Abcam, AB183612), p-tau (Abcam, AB151559), MBP (Abcam, AB40390), β-actin (Abcam, AB8226), or GAPDH (Abcam, AB181602) and mouse or rabbit secondary antibody (LI-COR IRDye 800CW) were used. Data quantification was performed by ImageJ software.

### Confocal microscopy imaging

For cellular uptake assay, Neuro-2a cells were cultured on microscope slides in 24-well plates ($1 \times 10^5$ cells per well) and incubated with NP@FAM-siRNA, Gal-NP@FAM-siRNA, or naked FAM-siRNA in 500 μl of medium (200 nM FAM-siRNA) at 37°C. The culture medium was removed, and the cells were washed three times with PBS, fixed with 4% paraformaldehyde solution for 15 min, and washed three times with PBS. Cells were then permeabilized with 0.1% Triton X-100 in PBS for 15 min and then stained with a tetramethyl rhodamine isothiocyanate (TRITC) fluorescent phalloidin conjugate solution (10 μg/ml) in PBS (containing 1% dimethyl sulfoxide from the original stock solution) for 30 min at room temperature and washed three times with PBS. The cell nuclei were stained with 4′,6-diamidino-2-phenylindole (DAPI) for 10 min and washed three times with PBS. The fluorescence images were obtained using a confocal microscope (Zeiss 880).

For endosomal escape, Neuro-2a cells were cultured on microscope slides in 24-well plates ($1 \times 10^5$ cells per well) and incubated with Gal-NP@FAM-siRNA in 500 μl of medium (200 nM FAM-siRNA) at 37°C for 2, 4, 6, and 8 hours. At the determined time, the culture medium was removed and the cells were washed three times with PBS and incubated with LysoTracker (50 nM, Invitrogen) at 37°C for 30 min and then with Hoechst 33342 (Solarbio, 10 μg/ml) for 10 min to visualize the endosomes/lysosomes and nuclei. Thereafter, cells were washed three times with PBS and fixed with 4% paraformaldehyde solution for 15 min. Fluorescence images were obtained using a confocal microscope (Zeiss 880).

For tissue immunofluorescence, brains were fixed in 4% paraformaldehyde for 24 hours, then dehydrated, embedded, and cut into 8-μm frozen slices. The sections were washed three times with PBS, blocked with normal goat serum for 1 hour, and subsequently incubated with anti–β-amyloid primary antibody (1:200, BioLegend, catalog no.803001) or anti-BACE1 primary antibody (1:250, Abcam,

AB183612) overnight at 4°C. Sections were then washed three times with PBS, and the slices were incubated with fluorescein isothiocyanate (FITC)–conjugated goat anti-mouse immunoglobulin G (IgG) (1:200, Abcam) or FITC-conjugated goat anti-rabbit IgG (1:200, Jackson) for 1 hour at room temperature. Then, the slices were stained with DAPI (10 μg/ml) for 10 min. The fluorescence images were obtained using a confocal microscope (Zeiss 880), and fluorescence intensity was analyzed by ImageJ software.

### Blood biochemistry and blood routine examinations

Healthy Balb/c female mice at age 6 to 8 weeks were randomly divided into two treatment groups ($n$ = 3). PBS and Gal-NP@siScr (1 mg of siRNA equiv./kg) were intravenously injected into mice via the tail vein ($n$ = 3 per group). At prescribed time points after injection, blood was collected via eye socket bleeding. For blood biochemistry examination, whole blood was centrifuged at 800$g$ for 5 min to collect serum for analysis. Standard blood chemistry parameters were analyzed using a kit from Wuhan Servicebio Technology Co. Ltd. on an automated chemistry analyzer (Chemray 240 Rayto lnc.). Blood cell parameters were analyzed with an automated blood cell analyzer (BC-2800Vet-Mindray Inc.).

### Novel object recognition

The NOR test was performed according to published methods (*32*). The experimental apparatus was a polyethylene white rectangular open field box (50 cm by 50 cm by 50 cm). Habituation took place by exposing the animal to the experimental apparatus for 10 min in the absence of objects on the day before training. During the training phase, mice were placed in the experimental apparatus in the presence of two identical objects (odorless wood cuboid or pyramid was used to prevent mice from climbing onto the object, avoid mice preference and sitting on it) and were allowed to explore the object for 10 min. After 24 hours, mice were placed again in the apparatus, where this time one of the objects was replaced by a novel one. Mice were allowed to explore for 10 min. DI and PI were used to assess NOR; this index accounts for differences in exploration time. DI and PI are calculated as the time spent exploring (total exploration of at least 30 s, sniffing, trying to move, and front paw pushing the objects were defined as exploring, but not the time spent near the objects without investigation, or passing by the objects). Data were collected using tracking software, and manual scoring was used to assess behaviors from the videos. DI was calculated as the time spent exploring the novel object minus the time spent exploring the familiar object, divided by the total exploration time. PI was calculated as the proportion of total time spent exploring new or old object. [DI = $T_{novel} - T_{familiar}/(T_{novel} + T_{familiar})$, PI = $T_{novel}$ or $T_{familiar}/(T_{novel} + T_{familiar})$]. All DI values fall between −1 and +1, and PI values fall between 0 and 1.

### Nest construction

The nest construction experiment was adapted from published methods (*29*). Test mice were caged and housed one mouse per cage. A pad of paper, 1 cm thick, was available in the cage before the start of the test. On the first day of the test, three pieces of paper (5 cm by 5 cm, kitchen towel) were introduced inside the home cage to allow assessment of nest-building behavior. After 24 hours, the nest was photographed and scored as follows: 0 points, no paper towels at all; 1 point, paper towels scattered throughout the cage, but no obvious bite marks (indicating active nest construction); 2 points, paper towels are concentrated in the cage, but no obvious bite marks; 3 points, the paper towel was concentrated on one side or one corner with some bite marks; 4 points, most of the paper towels were bitten and gathered together. The paper, which was shredded into small pieces or full of holes, was defined as bitten. All results were scored blindly.

### Morris water maze

To evaluate spatial learning and memory, MWM was performed in accordance with standard protocols (*52*). The pool was divided into four quadrants (Fig. 4G), and on the wall of each quadrant, a different symbol (pentagram, square, triangle, and circle) was affixed to provide extra-maze spatial cues. The water temperature was kept at 22 ± 1°C, and highly dispersed food-grade titanium dioxide was added into water to aid animal tracking. All MWM experiments were carried out daily and, at the same time, in the afternoon. The experimental equipment was kept in a confined space without noise or strong light sources.

Mice were habituated to the room for 2 hours before the experiment. Each mouse was trained to find a hidden platform for five consecutive days with four trials per day, with a 20- to 30-min intertrial interval. The mice were put into the water with their heads facing the wall of the pool, and the platform was allocated randomly to one of the four quadrants. The time the animals took to find the platform was recorded. In the training sessions, if the latency to find the platform exceeded 60 s, the animals were guided to the platform and kept there for 10 s. Mice were trained for 5 days to find the platform. Twenty-four hours after training, the platform was removed and the 60-s probe test commenced. Animals were placed into the water facing the quadrant, which was opposite the target quadrant. The time spent in the target quadrant and number of crossing the platform location was recorded as an indicator of spatial memory.

### Statistical analysis

Results were analyzed by using GraphPad Prism software. Differences between two groups were assessed using unpaired $t$ tests. For multiple comparisons, statistical significance was analyzed using one-way analysis of variance (ANOVA), followed by Fisher's least significant difference post hoc test, which was used when comparing all the conditions. Statistical differences in behavioral data were determined using two-way repeated-measures ANOVA. The level of statistical significance was set at $P < 0.05$. $^{*}P < 0.05$ was considered significant, and $^{**}P < 0.01$ $^{***}P < 0.001$ were considered highly significant. All data were expressed as mean ± SEM unless otherwise indicated.

## SUPPLEMENTARY MATERIALS

Supplementary material for this article is available at http://advances.sciencemag.org/cgi/content/full/6/41/eabc7031/DC1

View/request a protocol for this paper from *Bio-protocol*.

## REFERENCES AND NOTES

1. G. Livingston, A. Sommerlad, V. Orgeta, S. G. Costafreda, J. Huntley, D. Ames, C. Ballard, S. Banerjee, A. Burns, J. Cohen-Mansfield, C. Cooper, N. Fox, L. N. Gitlin, R. Howard, H. C. Kales, E. B. Larson, K. Ritchie, K. Rockwood, E. L. Sampson, Q. Samus, L. S. Schneider, G. Selbæk, L. Teri, N. Mukadam, Dementia prevention, intervention, and care. *Lancet* **390**, 2673–2734 (2017).
2. Alzheimer's Disease International, *World Alzheimer Report 2019* (Alzheimer's Disease International, 2019), pp. 1–166.

3. J. Versijpt, Effectiveness and cost-effectiveness of the pharmacological treatment of Alzheimer's disease and vascular dementia. *J. Alzheimers Dis.* **42**, S19–S25 (2014).
4. M. Williams, Progress in Alzheimer's disease drug discovery: An update. *Curr. Opin. Investig. Drugs* **10**, 23–34 (2009).
5. R. Briggs, S. P. Kennelly, D. O'Neill, Drug treatments in Alzheimer's disease. *Clin. Med.* **16**, 247–253 (2016).
6. R. Li, K. Lindholm, L.-B. Yang, X. Yue, M. Citron, R. Yan, T. Beach, L. Sue, M. Sabbagh, H. Cai, P. Wong, D. Price, Y. Shen, Amyloid β peptide load is correlated with increased β-secretase activity in sporadic Alzheimer's disease patients. *Proc. Natl. Acad. Sci. U.S.A.* **101**, 3632–3637 (2004).
7. R. Vassar, BACE1 inhibitor drugs in clinical trials for Alzheimer's disease. *Alzheimers Res. Ther.* **6**, 89 (2014).
8. N. M. Moussa-Pacha, S. M. Abdin, H. A. Omar, H. Alniss, T. H. Al-Tel, BACE1 inhibitors: Current status and future directions in treating Alzheimer's disease. *Med. Res. Rev.* **40**, 339–384 (2019).
9. A. Stamford, C. Strickland, Inhibitors of BACE for treating Alzheimer's disease: A fragment-based drug discovery story. *Curr. Opin. Chem. Biol.* **17**, 320–328 (2013).
10. F. Prati, G. Bottegoni, M. L. Bolognesi, A. Cavalli, BACE-1 inhibitors: From recent single-target molecules to multitarget compounds for Alzheimer's disease. *J. Med. Chem.* **61**, 619–637 (2018).
11. S. O. Bachurin, E. V. Bovina, A. A. Ustyugov, Drugs in clinical trials for Alzheimer's disease: The major trends. *Med. Res. Rev.* **37**, 1186–1225 (2017).
12. M. Zheng, W. Tao, Y. Zou, O. C. Farokhzad, B. Shi, Nanotechnology-based strategies for siRNA brain delivery for disease therapy. *Trends Biotechnol.* **36**, 562–575 (2018).
13. O. Singer, R. A. Marr, E. Rockenstein, L. Crews, N. G. Coufal, F. H. Gage, I. M. Verma, E. Masliah, Targeting BACE1 with siRNAs ameliorates Alzheimer disease neuropathology in a transgenic model. *Nat. Neurosci.* **8**, 1343–1349 (2005).
14. L. Alvarez-Erviti, Y. Seow, H. Yin, C. Betts, S. Lakhal, M. J. A. Wood, Delivery of siRNA to the mouse brain by systemic injection of targeted exosomes. *Nat. Biotechnol.* **29**, 341–345 (2011).
15. P. Wang, X. Zheng, Q. Guo, P. Yang, X. Pang, K. Qian, W. Lu, Q. Zhang, X. Jiang, Systemic delivery of BACE1 siRNA through neuron-targeted nanocomplexes for treatment of Alzheimer's disease. *J. Control. Release* **279**, 220–233 (2018).
16. M. Zheng, Y. Liu, Y. Wang, D. Zhang, Y. Zou, W. Ruan, J. Yin, W. Tao, J. B. Park, B. Shi, ROS-responsive polymeric siRNA nanomedicine stabilized by triple interactions for the robust glioblastoma combinational RNAi therapy. *Adv. Mater.* **31**, 1903277 (2019).
17. H. S. Min, H. J. Kim, M. Naito, S. Ogura, K. Toh, K. Hayashi, B. S. Kim, S. Fukushima, Y. Anraku, K. Miyata, K. Kataoka, Systemic brain delivery of antisense oligonucleotides across the blood–brain barrier with a glucose-coated polymeric nanocarrier. *Angew. Chem. Int. Ed.* **59**, 8173–8180 (2020).
18. J. Xie, D. Gonzalez-Carter, T. A. Tockary, N. Nakamura, Y. Xue, M. Nakakido, H. Akiba, A. Dirisala, X. Liu, K. Toh, T. Yang, Z. Wang, S. Fukushima, J. Li, S. Quader, K. Tsumoto, T. Yokota, Y. Anraku, K. Kataoka, Dual-sensitive nanomicelles enhancing systemic delivery of therapeutically active antibodies specifically into the brain. *ACS Nano* **14**, 6729–6742 (2020).
19. Y. Anraku, H. Kuwahara, Y. Fukusato, A. Mizoguchi, T. Ishii, K. Nitta, Y. Matsumoto, K. Toh, K. Miyata, S. Uchida, K. Nishina, K. Osada, K. Itaka, N. Nishiyama, H. Mizusawa, T. Yamasoba, T. Yokota, K. Kataoka, Glycaemic control boosts glucosylated nanocarrier crossing the BBB into the brain. *Nat. Commun.* **8**, 1001 (2017).
20. G. W. Gould, G. I. Bell, Facilitative glucose transporters: An expanding family. *Trends Biochem. Sci.* **15**, 18–23 (1990).
21. J. Klepper, T. Voit, Facilitated glucose transporter protein type 1 (GLUT1) deficiency syndrome: Impaired glucose transport into brain—A review. *Eur. J. Pediatr.* **161**, 295–304 (2002).
22. K. Shah, S. DeSilva, T. Abbruscato, The role of glucose transporters in brain disease: Diabetes and Alzheimer's disease. *Int. J. Mol. Sci.* **13**, 12629–12655 (2012).
23. P. M.-U. Ung, W. Song, L. Cheng, X. Zhao, H. Hu, L. Chen, A. Schlessinger, Inhibitor discovery for the human GLUT1 from homology modeling and virtual screening. *ACS Chem. Biol.* **11**, 1908–1916 (2016).
24. Z. Liu, Z. Zhang, C. Zhou, Y. Jiao, Hydrophobic modifications of cationic polymers for gene delivery. *Prog. Polym. Sci.* **35**, 1144–1162 (2010).
25. L. Holcomb, M. N. Gordon, E. McGowan, X. Yu, S. Benkovic, P. Jantzen, K. Wright, I. Saad, R. Mueller, D. Morgan, S. Sanders, C. Zehr, K. O'Campo, J. Hardy, C.-M. Prada, C. Eckman, S. Younkin, K. Hsiao, K. Duff, Accelerated Alzheimer-type phenotype in transgenic mice carrying both mutant amyloid precursor protein and presenilin 1 transgenes. *Nat. Med.* **4**, 97–100 (1998).
26. D. R. Borchelt, T. Ratovitski, J. van Lare, M. K. Lee, V. Gonzales, N. A. Jenkins, N. G. Copeland, D. L. Price, S. S. Sisodia, Accelerated amyloid deposition in the brains of transgenic mice coexpressing mutant presenilin 1 and amyloid precursor proteins. *Neuron* **19**, 939–945 (1997).
27. D. Puzzo, L. Lee, A. Palmeri, G. Calabrese, O. Arancio, Behavioral assays with mouse models of Alzheimer's disease: Practical considerations and guidelines. *Biochem. Pharmacol.* **88**, 450–467 (2014).
28. M. Ohno, S. L. Cole, M. Yasvoina, J. Zhao, M. Citron, R. Berry, J. F. Disterhoft, R. Vassar, BACE1 gene deletion prevents neuron loss and memory deficits in 5XFAD APP/PS1 transgenic mice. *Neurobiol. Dis.* **26**, 134–145 (2007).
29. D. W. Wesson, D. A. Wilson, Age and gene overexpression interact to abolish nesting behavior in Tg2576 amyloid precursor protein (APP) mice. *Behav. Brain Res.* **216**, 408–413 (2011).
30. P. Jirkof, Burrowing and nest building behavior as indicators of well-being in mice. *J. Neurosci. Methods* **234**, 139–146 (2014).
31. M. Filali, R. Lalonde, Age-related cognitive decline and nesting behavior in an APPswe/PS1 bigenic model of Alzheimer's disease. *Brain Res.* **1292**, 93–99 (2009).
32. R. Zhang, G. Xue, S. Wang, L. Zhang, C. Shi, X. Xie, Novel object recognition as a facile behavior test for evaluating drug effects in AβPP/PS1 Alzheimer's disease mouse model. *J. Alzheimers Dis.* **31**, 801–812 (2012).
33. G. S. Bloom, Amyloid-β and tau: The trigger and bullet in Alzheimer disease pathogenesis. *JAMA Neurol.* **71**, 505–508 (2014).
34. L. M. Ittner, J. Götz, Amyloid-β and tau—A toxic *pas de deux* in Alzheimer's disease. *Nat. Rev. Neurosci.* **12**, 65–72 (2011).
35. S. Oddo, L. Billings, J. P. Kesslak, D. H. Cribbs, F. M. LaFerla, Aβ immunotherapy leads to clearance of early, but not late, hyperphosphorylated tau aggregates via the proteasome. *Neuron* **43**, 321–332 (2004).
36. X. Hu, J. Hu, L. Dai, B. Trapp, R. Yan, Axonal and Schwann cell BACE1 is equally required for remyelination of peripheral nerves. *J. Neurosci.* **35**, 3806–3814 (2015).
37. M. K. Desai, K. L. Sudol, M. C. Janelsins, M. A. Mastrangelo, M. E. Frazer, W. J. Bowers, Triple-transgenic Alzheimer's disease mice exhibit region-specific abnormalities in brain myelination patterns prior to appearance of amyloid and tau pathology. *Glia* **57**, 54–65 (2009).
38. T. Lammers, F. Kiessling, M. Ashford, W. Hennink, D. Crommelin, G. Storm, Cancer nanomedicine: Is targeting our target? *Nat. Rev. Mater.* **1**, 16069 (2016).
39. M. Torrice, Does nanomedicine have a delivery problem? *ACS Central Sci.* **2**, 434–437 (2016).
40. B. Shi, M. Zheng, W. Tao, R. Chung, D. Jin, D. Ghaffari, O. C. Farokhzad, Challenges in DNA delivery and recent advances in multifunctional polymeric DNA delivery systems. *Biomacromolecules* **18**, 2231–2246 (2017).
41. H. Yin, R. L. Kanasty, A. A. Eltoukhy, A. J. Vegas, J. R. Dorkin, D. G. Anderson, Non-viral vectors for gene-based therapy. *Nat. Rev. Genet.* **15**, 541–555 (2014).
42. G. Tosi, M. A. Vandelli, F. Forni, B. Ruozi, Nanomedicine and neurodegenerative disorders: So close yet so far. *Expert Opin. Drug Deliv.* **12**, 1041–1044 (2015).
43. D. G. Souza, B. Bellaver, G. S. Raupp, D. O. Souza, A. Quincozes-Santos, Astrocytes from adult Wistar rats aged in vitro show changes in glial functions. *Neurochem. Int.* **90**, 93–97 (2015).
44. Y. An, V. R. Varma, S. Varma, R. Casanova, E. Dammer, O. Pletnikova, C. W. Chia, J. M. Egan, L. Ferrucci, J. Troncoso, A. I. Levey, J. Lah, N. T. Seyfried, C. Legido-Quigley, R. O'Brien, M. Thambisetty, Evidence for brain glucose dysregulation in Alzheimer's disease. *Alzheimers Dement.* **14**, 318–329 (2018).
45. A. Montagne, Z. Zhao, B. V. Zlokovic, Alzheimer's disease: A matter of blood–brain barrier dysfunction? *J. Exp. Med.* **214**, 3151–3169 (2017).
46. A. Montagne, D. A. Nation, A. P. Sagare, G. Barisano, M. D. Sweeney, A. Chakhoyan, M. Pachicano, E. Joe, A. R. Nelson, L. M. D'Orazio, D. P. Buennagel, M. G. Harrington, T. L. S. Benzinger, A. M. Fagan, J. M. Ringman, L. S. Schneider, J. C. Morris, E. M. Reiman, R. J. Caselli, H. C. Chui, J. Tcw, Y. Chen, J. Pa, P. S. Conti, M. Law, A. W. Toga, B. V. Zlokovic, APOE4 leads to blood–brain barrier dysfunction predicting cognitive decline. *Nature* **581**, 71–76 (2020).
47. X. Gu, Q. Song, Q. Zhang, M. Huang, M. Zheng, J. Chen, D. Wei, J. Chen, X. Wei, H. Chen, G. Zheng, X. Gao, Clearance of two organic nanoparticles from the brain via the paravascular pathway. *J. Control. Release* **322**, 31–41 (2020).
48. R. Vassar, B. D. Bennett, S. Babu-Khan, S. Kahn, E. A. Mendiaz, P. Denis, D. B. Teplow, S. Ross, P. Amarante, R. Loeloff, Y. Luo, S. Fisher, J. Fuller, S. Edenson, J. Lile, M. A. Jarosinski, A. L. Biere, E. Curran, T. Burgess, J.-C. Louis, F. Collins, J. Treanor, G. Rogers, M. Citron, β-secretase cleavage of Alzheimer's amyloid precursor protein by the transmembrane aspartic protease BACE. *Science* **286**, 735–741 (1999).
49. R. Yan, M. J. Bienkowski, M. E. Shuck, H. Miao, M. C. Tory, A. M. Pauley, J. R. Brashier, N. C. Stratman, W. R. Mathews, A. E. Buhl, D. B. Carter, A. G. Tomasselli, L. A. Parodi, R. L. Heinrikson, M. E. Gurney, Membrane-anchored aspartyl protease with Alzheimer's disease β-secretase activity. *Nature* **402**, 533–537 (1999).
50. S. L. Cole, R. Vassar, The basic biology of BACE1: A key therapeutic target for Alzheimer's disease. *Curr. Genomics* **8**, 509–530 (2007).
51. Y. Uno, W. Piao, K. Miyata, K. Nishina, H. Mizusawa, T. Yokota, High-density lipoprotein facilitates in vivo delivery of α-tocopherol–conjugated short-interfering RNA to the brain. *Hum. Gene Ther.* **22**, 711–719 (2011).

52. P. Zhao, X. Qian, Y. Nie, N. Sun, Z. Wang, J. Wu, C. Wei, R. Ma, Z. Wang, G. Chai, Neuropeptide S ameliorates cognitive impairment of APP/PS1 transgenic mice by promoting synaptic plasticity and reducing Aβ deposition. *Front. Behav. Neurosci.* **13**, 138 (2019).

**Acknowledgments:** We thank K. Kataoka at University of Tokyo and R. Chung at Macquarie University for scientific discussions and suggestions. **Funding:** This work was supported by the National Natural Science Foundation of China (NSFC U1804139, U1604177, 31800841, 31922045, 31771031, and 81701829), National Key Technologies R&D Program of China (2018YFA0209800), Key Research Program in Colleges and Universities of Henan Province (19zx006), Australian Endeavour Fellowship (no. 69172018), Mason Foundation National Medical Program (MAS2017F034), National Health and Medical Research Council (NHMRC) Dementia Fellowship (GNT1111611), and NHMRC Project Grant (GNT1166024). **Author contributions:** M.Z., X.X., and B.S. designed the concept, supervised the project, and revised the manuscript. F.Z., Y.Zh., Y.L., Y.W., D.Z., Y.Zo., and H.W. performed the experiments and analyzed the data. M.Z. and F.Z. led the design, preparation, and functional characterization of nanocomplexes. X.X. and Y.Zh. led the animal experiments. M.Z. and Y.L. wrote the manuscript and revised it according to the comments of Y.A., O.S., A.I.B., J.L., X.P., W.T., Y.Zo., and B.S. All authors participated in the discussion of the project. **Competing interests:** The authors declare that they have no competing interests. **Data and materials availability:** All data needed to evaluate the conclusions in the paper are present in the paper and/or the Supplementary Materials. Additional data related to this paper may be requested from the authors.

Submitted 13 May 2020
Accepted 26 August 2020
Published 9 October 2020
10.1126/sciadv.abc7031

**Citation:** Y. Zhou, F. Zhu, Y. Liu, M. Zheng, Y. Wang, D. Zhang, Y. Anraku, Y. Zou, J. Li, H. Wu, X. Pang, W. Tao, O. Shimoni, A. I. Bush, X. Xue, B. Shi, Blood-brain barrier–penetrating siRNA nanomedicine for Alzheimer's disease therapy. *Sci. Adv.* **6**, eabc7031 (2020).